Journal of Power Sources 660 (2025) 238565

Contents lists available at ScienceDirect

Journal of Power Sources

journal homepage: www.elsevier.com/locate/jpowsour

Safety and performance implications of lithium plating induced by sub-zero temperature cycling of lithium-ion batteries

Charles Kirchner-Burles [a,b,e], Arthur Fordham [a,e], Hamish T. Reid [b], Michael Johnson [a,e], Mark Buckwell [b], Francesco Iacoviello [a], Kofi Coke [a,e], Rhodri Jervis [a,e], Gareth Hinds [d], Paul R. Shearing [c,e,*], James B. Robinson [a,b,e,**]

[a] Electrochemical Innovation Lab, Department of Chemical Engineering, University College London, London, WC1E 7JE, UK
[b] Advanced Propulsion Lab, Marshgate, University College London, London, E20 2AE, UK
[c] ZERO Institute, Holywell House, Osney Mead, University of Oxford, Oxford, OX2 0ES, UK
[d] National Physical Laboratory, Hampton Road Teddington Middlesex TW11 0LW, UK
[e] The Faraday Institution, Quad One, Becquerel Avenue, Harwell Science and Innovation Campus, Didcot, OX11 0RA, UK

HIGHLIGHTS

- Degradation and safety of Li-ion cells at low temperatures examined.
- Influence of temperature on Li plating on safety explored.
- Jelly roll collapse due to Li-plating observed.
- Multi-technique characterisation details increased safety risk at low temperatures.

ABSTRACT

The operation of lithium-ion cells at sub-zero temperatures can result in the deposition of metallic lithium onto the surface of the negative electrode. The resulting lithium deposits have substantial ramifications for the performance and safety of the cell, with rapid capacity fade and reduced thermal stability both exhibited in cells aged under these conditions. In this study, it is found that extending the cycling temperatures of these cells to sub-zero temperatures results in a change in plating behaviour, with cells cycled at −10 °C exhibiting reversible plating behaviour and cells cycled at −20 °C plating irreversibly instead. Additionally, the nature of the plating is observed to transition from reversible to irreversible with progressive ageing in the cells cycled at −10 °C. Using *operando* electrochemical analysis such as voltage relaxation and Coulombic efficiency (CE) measurement, characteristics of the degradation are revealed. Electrochemical impedance spectroscopy (EIS) is also employed between cycles to provide information on the changes in internal cell processes due to plating. *Ex-situ* investigations complement the analysis allowing images of electrode condition to be collected. *In-situ* X-ray computed tomography further highlights how lithium plating compromises the structural integrity of the internal cell architecture, leading to increased safety concerns. Testing the aged cells with accelerated rate calorimetry also shows that the presence of more strongly reductive metallic lithium within a cell results in lower onset temperatures for self-heating and thermal runaway, plus an increased potential for projectiles during failure.

1. Introduction

Lithium-ion batteries have become the technology of choice for energy storage, with applications ranging from consumer electronics to electric vehicles [1]. Their versatility and growing demand have required ongoing improvements to cell energy densities and safe operation in increasingly severe conditions. One condition that is particularly influential on the state of health of a battery is sub-zero temperature. Cold cycling has been shown to substantially impact cell performance and increase the risk of catastrophic failure [2–4]. Large parts of the world and many specialised applications, such as aerospace, military equipment, and polar research, require batteries to function over long lifetimes in sub-zero temperatures [4]. To accommodate these more challenging environments, it is important to fully understand the degradation behaviour and safety characteristics of cells.

The lifetime performance of a cell is influenced by the extent of

* Corresponding author. ZERO Institute, Holywell House, Osney Mead, University of Oxford, Oxford, OX2 0ES, UK.
** Corresponding author. Advanced Propulsion Lab, Marshgate, University College London, London, E20 2AE, UK.
E-mail addresses: paul.shearing@eng.ox.ac.uk (P.R. Shearing), j.b.robinson@ucl.ac.uk (J.B. Robinson).

https://doi.org/10.1016/j.jpowsour.2025.238565
Received 24 January 2025; Received in revised form 16 September 2025; Accepted 1 October 2025
Available online 8 October 2025

degradation it undergoes. Degradation is a complex and interconnected process which involves several contributary modes including the loss of lithium inventory, loss of active material, stochiometric drift and increase of cell impedance [5–8]. Understanding the mechanisms for these modes of degradation is essential for ensuring durability and safe operation of lithium-ion batteries.

Catastrophic failure in a cell can be initiated via three main modes: mechanical, electrical and thermal. Mechanical failure mostly occurs due to an external force deforming the internal architecture of the cell, inducing a short circuit within the cell [9]. However, in some cases the deformation force can come from within the cell, as will be shown in the discussion and by prior work [10]. Cells can undergo parasitic reactions over time, generating both gaseous and solid by-products, such as metallic lithium deposits and additional Solid Electrolyte Interphase (SEI) growth. These solid species increase the thickness of the electrode layers, creating internal pressure within the cell. Combined with gas buildup, this can lead to the deformation of the inner electrode assembly in cylindrical cells, causing it to collapse or fold. Such structural changes compromise the mechanical integrity of the "jelly roll" design, increasing the risk of internal short circuits and potential cell failure [11]. Whilst the current literature extensively covers how lithium plating diminishes the electrochemical performance of a lithium-ion cell [12–15], the impact of plating on the mechanical integrity and thermal stability of a cell is not yet fully understood. Carter et al. found that lithium plating, in cells without a central mandrel, was not the sole reason for capacity fade at sub-zero temperatures; mechanical deformation can result in contact loss and electrical isolation, contributing to performance decay [16].

Thermal runaway can also be induced electrically, through connecting the positive terminals internally or externally, otherwise referred to as a short circuit. It is widely recognised that internal and external short circuits (ISCs/ESCs) are amongst the primary causes of thermal runaway. Fire statistics in EVs highlight that 52 % of major failures involve ISCs and a further 26 % involve ESCs [17–19]. A short circuit occurs when a negative and a positive component make a connection. Whilst ESCs can be mitigated by managing the external operating environment of a cell, ISCs are harder to predict and prevent. Most commonly, they occur when lithium metal is deposited onto the graphite negative electrode forming dendrites that penetrate the separator creating an electrical pathway [20,21]. These short circuits dissipate large amounts of energy into the local cell environment, heating material in the proximity and potentially triggering a thermal runaway event [14,22–24].

Lithium plating arises when conditions of negative overpotential with respect to Li/Li^+ are induced at the graphite electrode surface. These conditions can be created by overcharging, high charging currents, or sub-zero temperature operation [25]. As the temperature reduces, the negative electrode is subjected to large overpotentials at the electrode surface due to slower solid-state diffusion within the graphite [26]. This reduced diffusion causes the blocking of interstitial sites at the surface as they become saturated with intercalating Li-ions faster than they can diffuse into the bulk electrode [27], causing significant polarisation at the graphite surface. The negative electrode potential vs Li/Li^+ then drops below 0, which causes the deposition of metallic lithium [28,29] to become thermodynamically favourable over lithium-ion intercalation [14,30], resulting in the loss of lithium inventory and a corresponding reduction in CE and capacity of the cell.

Cells may also be induced into failure via thermal abuse. When a cell is heated, the SEI and electrolyte begin to break down and reform in exothermic reactions, generating internal heat. This increase in temperature accelerates the decomposition of active materials, releasing additional heat and oxygen. These exothermic reactions cause self-heating, which can trigger a cascade of reactions, leading to further heat generation. This self-sustaining cycle can result in thermal runaway, where rapid heat buildup ultimately leads to cell failure. This mode is usually initiated by an external heat source, e.g. fire or a circuit malfunction, or via the other modes of failure such as a short circuit, which will generate the heat required to kickstart this feedback loop [31].

Lithium plating can be reversible or irreversible. Reversible lithium plating occurs when the deposited metallic lithium remains in electrical contact with the negative electrode, so that current can still flow across these deposits and engage in stripping [32]. However, with irreversible plating the metallic lithium deposited during the plating process loses this electrical contact and therefore cannot engage in stripping, meaning it is no longer accessible. This is referred to as 'dead' lithium, which can then accumulate at the surface blocking the active sites from Li-ion intercalation. Even if Li-ions do manage to intercalate past the 'dead' lithium this pathway is often more tortuous, which further adds to the increasing cell impedance [33]. Being able to identify which plating mode is occurring during cell degradation is crucial for understanding performance decay at sub-zero temperatures.

To accurately monitor the development of lithium plating during a cell's operation, a litany of techniques has been employed. Uhlmann et al. investigated lithium plating by observing the open circuit potential (OCP) of a half-cell after different charging currents were applied. When higher currents were used for charging, a double plateau featured on the relaxation profile of the OCP as a result of lithium stripping [34]. Schindler et al. proposed the idea that the width of the plateau could provide quantitative estimations of the amount of plated lithium, something that was proved by work from Von Lüders et al. using *in-situ* neutron diffraction [35,36]. The electrochemical processes within the cell are directly impacted by lithium plating and so measuring the changes in electrochemical parameters, such as voltage, capacity, impedance, and CE, we can see these effects. Burns et al. utilised High Precision Coulometry as a method of detecting plating. Reductions in cycling efficiencies were detected at high charging rates which was attributed to plating. They varied the temperature of these experiments to find that minor drops in CE occur as active lithium is consumed by this parasitic reaction [37]. These passive detection methods allow for measurements to be taken *operando*. Lithium plating, whether reversible or irreversible, will affect a cell's electrochemical parameters differently. When in electrical contact, metallic lithium can be stripped off, forming lithium-ions in a process that contributes to cell capacity and voltage [38]. Monitoring these parameters enables us to indirectly observe this stripping process competing with electrode relaxation. To reveal signs of irreversible plating it is necessary to study the changes in CE and cell impedance [37]. Petzl et al. used EIS to track changes in Ohmic resistance in cells aged at sub-zero temperature. The study found that increases in Ohmic resistance were indicative of lithium plating due to the irreversible consumption of lithium inventory and electrolyte solvents, which decreased the ionic conductivity of the electrolyte [39]. The 'dead' lithium impedes migratory and intercalation processes but also deducts from the lithium inventory.

This paper analyses the electrochemical performance of lithium-ion cells aged at different temperatures, focusing on capacity retention, degradation rates, and CE. *In-situ* diagnostic tools are used to investigate the underlying mechanisms of performance loss. While lithium plating is widely recognised as the main cause of degradation at low temperatures, most studies focus only on its presence and severity. There is limited research exploring how temperature influences the nature of plating—specifically, whether it is reversible or irreversible. This work aims to address that gap by investigating the conditions that govern this distinction, and the ramifications it has on cell safety.

2. Experimental

This investigation utilised cylindrical 21700 Molicel P42A cells (E-One Moli Energy, Taiwan) throughout, which have 4.2 A h rated capacity. The cell chemistry consists of a graphite and SiO_x negative electrode, a polymer separator, and a nickel cobalt aluminium (NCA) metal oxide positive electrode. The cells are rated for a voltage range of 2.5–4.2 V. The cells are designed for high-power applications and are

capable of discharge at 45 A and charging at 4.2 A. A symmetrical 1C (4.2 A) charge/discharge protocol was chosen to age the cells. In total, 12 cells were initially charged at 4.2 An until they reached a voltage of 4.2 V, following which a constant voltage of 4.2 V was applied until the current tapered to a cut-off value of 50 mA. They were then discharged at 4.2 An under constant current until the lower voltage cut-off limit, 2.5 V. The cells were aged over 50 cycles as so to reduce the severity of the degradation of the cells aged at sub-zero temperatures, and thus the risk of the experiment. During these cycling tests three cells were held at each of the three different temperatures: room temperature (*ca.* 25 °C), −10 °C, and −20 °C in environmental chambers (LabEvent Benchtop Temperature Test Chamber, Weiss-Technik) as shown in Table 1. Cell temperatures were monitored using a K-type thermocouple connected to the battery cycler, positioned at the midpoint of the cell's outer surface to approximate internal temperature. Ageing was tracked using a battery cycler (BCS-815 system, BioLogic) which also performed electrochemical impedance spectroscopy (EIS) on the cells between 10 kHz and 10 mHz using a 60 mA perturbation. This was carried out following the relaxation period described in Fig. 4. Each cell is left to rest at open circuit potential for a period of 2 h, for the room temperature cells, which was extended to 3 h for the cells aged at −10 °C and 5 h for the cells aged at −20 °C.

Cells 8 and 9 did not finish the 50-cycle ageing regime as the cells shorted during the cycle number shown below in Table 1.

Following the ageing protocol, one cell from each set (Cells 10–13 – including a pristine cell) was discharged (1C at constant current) to a safe operation voltage (3.3 V – lower potentials can lead to copper dissolution at the anode [40]) before being safely disassembled in a glovebox (UNIlab pro glovebox system, MBRAUN) under an argon atmosphere for *ex situ* characterisation of the electrodes. Of these cells, 3 underwent a tear-down analysis which was used to study the electrodes' physical condition. The pristine cell was also opened to provide a 'fresh' condition electrode as a reference. The harvested electrodes were then washed with dimethyl carbonate (DMC) (anhydrous, >99.5 %, Sigma Aldrich) and dried before preparing samples using ceramic scissors and removing from the glovebox. Sample sizes for scanning electron microscopy (SEM) were kept close to 1 cm × 1 cm and for optical microscopy (VHX-7000 Digital Optical Microscope, Keyence) the sizes varied more but were generally *ca.* 10 cm × 3 cm. These samples were imaged using a scanning electron microscope (EVO MA 10, Zeiss) using the SE1 signal and 10 kV accelerating voltage, at a working distance of 8.5 mm. It should be noted that during the transfer of these samples from the glovebox to the imaging stages of various instruments, they were exposed to air and moisture. This exposure means that any lithium present in the samples likely reacted with moisture to form lithium hydroxide (LiOH). Such reactions can alter the sample's surface chemistry, potentially affecting the accuracy of the imaging and analysis results by introducing additional lithium compounds that were not originally present in the controlled glovebox environment.

Table 1
Summary of the ageing parameters of the cells and where they were used in the analysis.

Cell Label	Operating Temperature (°C)	Number of Cycles	Experiment
1	25	50	ARC
2	25	50	Cycling
3	25	50	Cycling
4	−10	50	ARC
5	−10	50	Cycling
6	−10	50	Cycling
7	−20	50	ARC
8	−20	32	Cycling
9	−20	36	Cycling
10	Pristine	0	Tear Down
11	25	50	Tear Down
12	−10	50	Tear Down
13	−20	50	Tear Down

A lab-based macro–X-ray CT system (NIKON XT 225, Carl Zeiss XRM) was used to acquire tomographic reconstructions of the cells before and after ageing, as well as post-failure. Each radiographic scan was taken with a 1 mm copper filter and at an accelerating voltage of 210 kV with a tungsten target, generating 2027 projections with pixel resolution of 32 μm. The resulting datasets were reconstructed using the CT Pro 3D software with a built in filtered back projection algorithm then subsequently visualised using Avizo Fire 2024.2 (Thermo Scientific).

The thermal abuse tests used to study the thermal stability of the aged cells were performed using accelerating rate calorimetry (THT ES, Thermal Hazard Technology). The heat-wait-search protocol used a starting temperature of 50 °C and incrementally stepped up the temperature in discrete 5 °C steps before waiting for any thermal transients to decay. If temperature remains unchanged (using a 0.005 °C min^{-1} sensitivity) then heating continues until self-heating is detected. Cell temperatures were recorded using a N-type thermocouples that were attached to the cap, along the midpoint of the cell surface, and at the base of the cell.

3. Results

The sub-zero temperature ageing results shown in Fig. 1 indicate a significant loss in cell performance over relatively short cycling durations with clear capacity loss for each ageing temperature. As expected, the cells cycled at room temperature exhibited relatively consistent performance behaviour over the 50 cycles, with average capacity losses limited to 5 % through these early cycles. This capacity loss is most likely due to cycling at 1C which is a relatively high C-rate.

It is worth noting that throughout the ageing regime, the environmental chamber temperature was maintained, but the internal cell temperature rose during cycling due to Ohmic heating and polarisation losses [41], see SI Figures S3-5, due to the high C-rates used. While this introduces some deviation in the measured variables, it is considered acceptable as it reflects real-world operating conditions, where internal cell temperatures are typically higher than the ambient environment.

The largest temperature rise consistently occurred during discharge—a phase not directly associated with lithium plating. However, since stripping is strongly temperature-dependent, as described by the Arrhenius relationship [42], even modest heating must be considered. For both sub-zero ageing conditions, peak internal temperatures reached around 0 °C, rising ~10 °C at −10 °C and ~19 °C at −20 °C. Although the cells are at the same overall temperature, there is a larger temperature rise in the cells at −20 °C. This greater temperature rise is most likely attributed to increased internal resistance at lower temperatures and reflects a realistic cell response. As a result, the colder cells are expected to have relatively higher capacity recovery due to thermal effects, compared to the cells at −10 °C.

During charging, temperature rises were modest (~6 °C and ~7 °C at −10 °C and −20 °C, respectively), and occurred early in the process, with the cell returning close to its open-circuit potential (OCP) temperature average by the later stages which is where lithium plating is most prominent. Therefore, the influence of cell heating on plating behaviour during charge is assumed to be consistent across the temperature range.

While this initial degradation is relatively high for a cell which has a rated lifetime of *ca.* 500 cycles under normal operation conditions (25 °C) as outlined in the cell specification sheet, it has been previously observed that capacity drops comparatively quickly in early cycles before stabilising for subsequent cycles due to the formation and thickening of the SEI layer [43].

As the operational temperature is reduced, capacity fade over the duration of the cycling tests can be seen to increase with average losses of 43 % and 70 % observed at temperatures of −10 °C and −20 °C, respectively. This reduction in performance is likely to be caused by substantial Li plating, known to occur at sub-zero temperature operation [26]. The plating of metallic Li results in the loss of lithium inventory

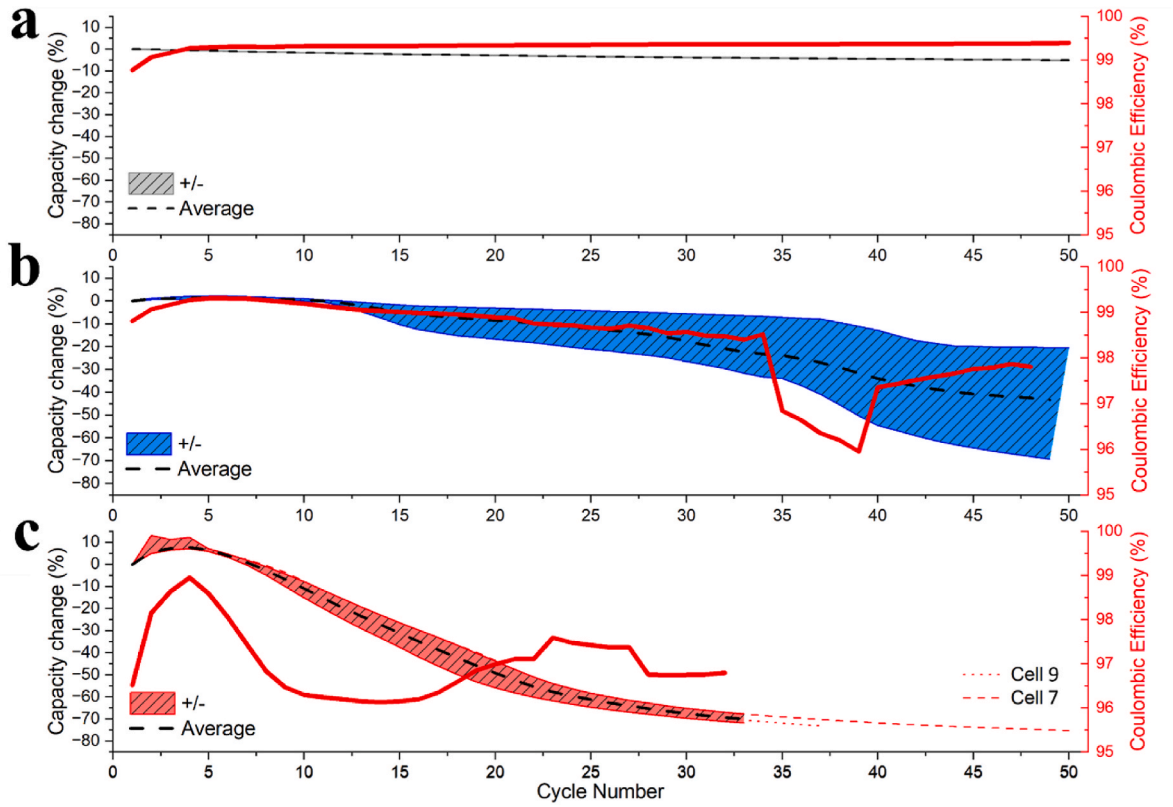

Fig. 1. The discharge capacity losses for each ageing regime: (a) room temperature, (b) −10 °C, and (c) −20 °C. Each curve represents the mean of three cells per ageing set, with the mean and associated error smoothed using a 5-point rolling average. The right-hand axes display the corresponding mean Coulombic efficiencies, also presented with a 5-point rolling average. For the −20 °C ageing regime, two cells reached their cycling safety limits and were terminated prior to 50 cycles; the individual curves are shown extended beyond this point.

reducing the cells CE and capacity. The results shown here align with previously reported literature which indicates that further reduction to the operating temperature exacerbates these overpotentials and produces higher levels of metallic lithium deposition [34], as indicated by the higher capacity loss seen in Fig. 1.

Fig. S1 shows that, while room temperature cells age at a relatively uniform rate, the reduction in temperature produces significant variations in the ageing rate. Cells aged at −10 °C can be seen to show slow increases in capacity decay, with a maximum rate of decay observed at Cycle 38. In contrast, the cells aged at −20 °C show maximum decay rates after 10 cycles and remain high until 20 cycles. Beyond the minima observed the rate of capacity loss declines towards zero, indicating that at this stage a stable metallic lithium layer has formed across the surface of the negative electrode. Broussely et al. reported that lithium plating is a self-reinforcing process with precipitated lithium blocking the pores of the electrode which reduces the porosity, a recognised first-order parameter of performance [44]. This process also decreases the active surface area of the negative electrode, resulting in local increases in current density across the remaining unblocked electrode interface, further encouraging plating [28,44].

It can also be seen in Fig. 1 and Fig. S1 that a temporary increase in the discharge capacity delivered by the cells cycled at cold temperatures is observed during the first 5 cycles. The effect is more pronounced in the cells cycled at −20 °C. This is likely due to the active material becoming more brittle at sub-zero temperatures with an increased rate of electrode cracking and a subsequent increase in electrode surface area experience during operation. This, in turn, may provide a temporary increase in capacity until plating becomes established [45]. This capacity increase could also be contributed to by internal heating within the cell from joule heating. Further evidence for this process can be found in the EIS data discussed later that shows an initial drop in resistance, especially with processes associated with the SEI. Despite this, more information is needed to fully assign a cause of the apparent initial increase in capacity.

Another notable difference between the cell performance of each ageing set is the initial capacities (cycle 1). The cells under ambient conditions registered an average capacity of *ca.* 4000 mA h, whilst the cells aged at −10 °C and −20 °C produced average initial capacities of *ca.* 3300 mA h and 2800 mA h, respectively. These cells have been in storage for 6 months, which is why the cells have lower initial capacities than those quoted on the spec sheet (3800 mA h at −20 °C). The discharge capacity seen in the ambient cells is towards the lower end of the range of variance stated in the specification sheet for this model of cell. The reduced initial capacity in the cold cells is primarily attributed to the reduced kinetics of the internal electrochemical processes. At sub-zero temperatures the conductivity of the electrolyte is significantly reduced, charge transfer is sluggish, the SEI has increased resistance, and Li ion diffusion through the bulk material is slow [46].

Fig. 2 highlights the voltage behaviour of each of the nine cells, which provides an insight into the nature of the degradation during the sub-zero temperature testing. It is clear, as shown previously in Fig. 1, that capacity fade is observed as the cells are cycled, with lower capacities generally delivered as the temperature is reduced.

Large overpotentials were observed during both charge and, to a lesser extent, discharge, with the effect most pronounced at −20 °C. During charging, these overpotentials were sometimes so severe that they prematurely triggered the constant-voltage (CV) stage above 4.2 V, significantly reducing charging capacity. The origin of such behaviour lies in the sluggish lithium-ion transport and intercalation kinetics at reduced temperatures, as described by the Arrhenius relationship, which increase the resistance to charge transfer and ion diffusion [42,47]. With cycling, structural and electrochemical degradation compounds this effect: SEI growth, loss of active material, and rising interfacial

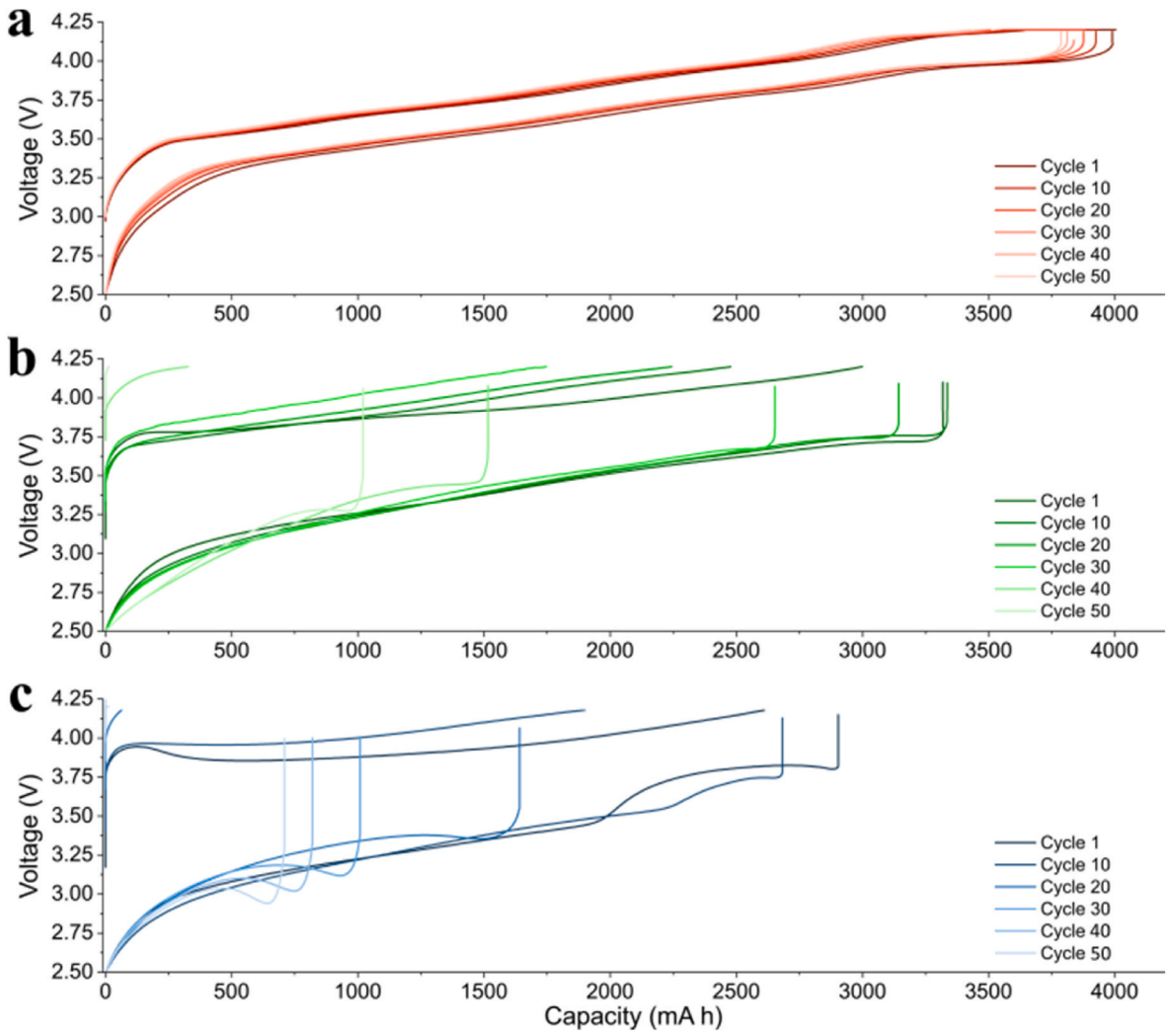

Fig. 2. The voltage profiles of cells aged at ambient temperatures (~25 °C) (a), −10 °C (b), and −20 °C (c), over selected cycles of the ageing protocol. The data sets are represented by cells 1, 4 and 7, with voltage profiles for the remaining cells provided in the Supporting Information (Fig. S2).

resistance from charge-transfer processes all exacerbate overpotentials [48]. Critically, lithium plating becomes increasingly favoured under these kinetic limitations, particularly during the constant-current (CC) charging phase, where the high overpotential drives Li deposition on the graphite surface rather than intercalation [49]. The subsequent formation of metallic and 'dead' lithium further impedes ion transport across the electrode–electrolyte interface, accelerating the voltage rise. In two cells aged at −20 °C, the overpotentials became so large that the terminal voltage exceeded the upper safety cut-off of 4.25 V after only ~35 cycles, triggering automatic termination of cycling to mitigate the risk of internal short circuit or thermal runaway.

These results highlight the detrimental effects of low temperature cycling on cell performance but offer limited insight into the underlying mechanisms. To better understand why and how these losses occur, in-situ analytical techniques are employed. These methods provide valuable information on changes in cell impedance, phase transitions, voltage relaxation behaviour, and the evolution of key electrochemical processes during ageing.

Performing EIS on the aged cells highlights how their impedance changes with ageing (see SI for full set of spectra: S6). This is an effective tool for understanding the extent and nature of any degradation occurring within a cell. Certain modes of degradation cause increases in impedance or resistance for specific processes. For lithium plating, we expect to see increases in impedance for charge transfer between the electrolyte and negative electrode, due to the growing layer of lithium increasing the tortuosity of ion-transport and blocking active sites for intercalation. Impedance of the SEI also rises as lithium's higher reduction potential means that plating results in thicker and more voluminous SEI layers. Lastly, loss of lithium inventory from the electrolyte, due to plating, causes a drop in ionic conductivity and thus an increase in Ohmic resistance. These are the features that will be analysed to assess the extent of plating. The temperature of these experiments was maintained to avoid any material expansion due to temperature changes that could result in potential capacity recovery or further mechanical degradation (cracking, etc.). This means that EIS was also recorded at sub-zero temperatures which gives rise to inherent impedance contributions from the reduced electrochemical and physical kinetics of cell operation, and the lower resistances from metallic components within the cell at sub-zero temperatures affect the EIS results versus that of cells aged at room temperature. Both Ohmic resistance and ionic conductivity are both temperature dependent, with the later directly influencing cell impedance. This means comparisons between these cells, in terms of their impairment to nominal function, is difficult, as the cells at lower temperatures will intrinsically have higher impedance. Despite this, changes in key parameters remain comparable and have been summarised in Fig. 3: R_b represents the ohmic resistance of the cell, R_{SEI} represents the impedance associated with the SEI, and R_{ct} represents the impedance associated with charge transfer.

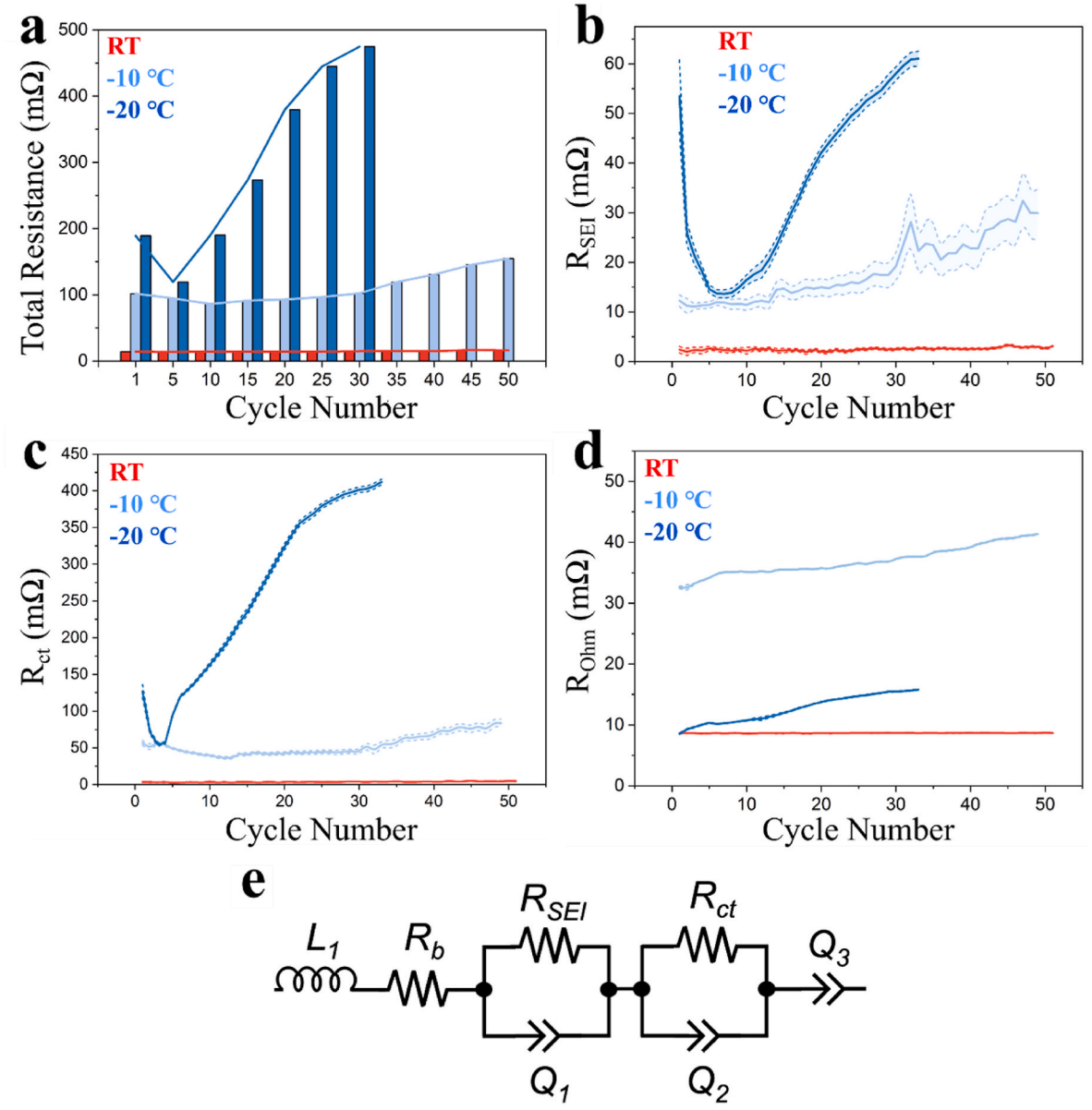

Fig. 3. The changes in impedance experienced by the aged cells. For each ageing temperature, the average response is used to represent the following impedance parameters: (a) total resistance; (b) impedance associated with the SEI; (c) impedance associated with charge transfer; and (d) Ohmic resistance. These measurements are derived from the equivalent circuit model shown in (e). The corresponding fittings and associated errors are provided in the Supporting Information (Tables 1–3). Full spectra can be found in the SI, see S6.

The cells aged at room temperature exhibit a consistent level of impedance throughout ageing, shown in Fig. 3a, which displays the cell's total resistance, which is also reflected in the resolved spectra for each of the associated electrochemical processes discussed above. In contrast, the cells operated at reduced temperatures in general show an initial drop in impedance (SEI and CT associated) followed by a steady increase with cycling in impedance associated with the SEI, (Fig. 3b), charge transfer, (Fig. 3c), and Ohmic resistance, (Fig. 3d). In keeping with the ageing trends shown previously, the colder cells, cycled at −20 °C, show more significant increases in total impedance during the early phases of ageing (*ca.* 125 mΩ at cycle 5 to *ca.* 450 mΩ at cycle 30) with the cells at −10 °C showing similar increases later in cycling – cell resistance stays stable at *ca.* 100 mΩ before rising to approximately 150 mΩ after cycle 50. There is also a clear initial drop in SEI and charge transfer impedance in these cold cells (especially those aged at −20 °C), which was earlier attributed to particle cracking features that occur due to the expansion and contraction of the brittle electrode material at sub-zero temperatures creating cracks that initially increase the active surface area of the graphite electrode. This appears to happen within the first ten cycles or so, and then impedance increases as would be expected – most likely because the cracks become surrounded by new SEI. These increases in impedance are more significant in the cells at −20 °C, with charge transfer impedance increasing from 50 mΩ in cycle 3–410 mΩ after cycle 33, and impedance associated with the SEI increasing from 15 mΩ in cycle 6–60 mΩ after 33 cycles. This increase can be attributed to the irreversibility of the lithium plating at these temperatures compared to the cells at −10 °C, which experiences increases in charge transfer and SEI impedance of 25 mΩ and 15 mΩ respectively. Ohmic resistance appears to rise comparatively (*ca.* 7 mΩ) in both the sub-zero temperature ageing sets, although this is difficult to deconvolute due to the competing effects of temperature on electronic and ionic resistance, implying that in each case there are similar drops in ionic conductivity due to losses in lithium inventory but over a shorter ageing period for the cells at −20 °C. The Ohmic resistance for the cells at −20 °C is lower

than the cells at −10 °C due to the lower resistivity of the metal components (current collectors, wires, etc.) of the cell.

The voltage relaxation profiles, in Fig. 4, offer interesting insights into the stripping behaviour during cold ageing. After charging, the negative electrode undergoes relaxation, a process which results in a drop in voltage. When reversible lithium plating is present, stripping can occur, pushing the voltage in the opposite direction. These two processes compete until all the reversible lithium available is stripped off the graphite surface and relaxation mechanics take over. This transition of mechanisms results in a double plateau in the relaxation profile of the open circuit potential where the inflection point between these two plateaus indicates the end of lithium stripping [14,15,50]. As expected, conventionally aged cells exhibited no signs of the double plateau characteristic of Li plating; in contrast, at −10 °C a double plateau feature that migrates across the plot with ageing can clearly be observed. By examining the derivative of this plot, also found in Fig. 4, the shift of the plating behaviour can be seen more clearly. The inflection points of the double plateau occur in shorter time periods as the cells age (this observation is summarised in a graph in the SI, see Fig. S7). Based on this evidence, lithium stripping appears to become less significant due to a reduced extent of reversible plating. As metallic lithium layers thicken, less of the lithium is in electrical contact and so cannot engage in stripping as easily [51]. Furthermore, parasitic reactions between the metal lithium and the electrolyte can cause the lithium layer to break apart and become isolated from the graphite electrode. As well as this, the ageing rate discussed earlier shows that degradation continues to increase beyond when the shift in the differential voltage peaks begins to stagnate (*ca.* Cycle 10). This suggests a shift from reversible lithium plating mechanisms to more irreversible ones.

Interestingly, the relaxation profiles of the cells cycled at −20 °C do not exhibit any double plateau features. The absence of this is likely due to the irreversible nature of the lithium plating inhibiting any stripping from occurring. The sub-zero temperature likely causes stripping behaviour to become energetically unfavourable, thus no contributions to the capacity from recovered metallic lithium are seen. Fig. 1 also supports the irreversibility of lithium plating at this temperature; the accumulation of 'dead' lithium causes the CE of the cell to drop, whereas metallic lithium capable of engaging in lithium stripping will still contribute to the capacity of the cell and so not resulting in a decline in CE.

The CEs of the cells shown in Fig. 1, also provide information on the extent of irreversible plating. As plating arises, the CE of the cell drops since a portion of the lithium plated during charging becomes electrically isolated and cannot be accessed during discharge, contributing to capacity loss. The ambient cells, in which no plating occurs, show consistent efficiencies close to 100 %, whereas the colder cells show significantly reduced, and variable CEs. These behaviours again reflect the ageing rates that were discussed previously. The cells at −20 °C show greater drops in CE during the early cycles and the cells at −10 °C are seen to peak at approximately 30 cycles. In the cells aged at −10 °C, the CE begins to decline concurrently with the disappearance of the double-plateau feature (ca. Cycle 10), at which point the ageing rate also becomes negative (see S1). This behaviour is characteristic of irreversible capacity loss and strongly suggests that lithium plating has transitioned from a partially reversible to an irreversible process. The likely cause is the progressive accumulation of metallic lithium and SEI growth at the graphite surface, with increasing thickness and density of these layers rendering portions of plated lithium electrochemically inaccessible [12–14]. This effect is further exacerbated by the high reactivity of lithium with the electrolyte, which accelerates parasitic side reactions and contributes to the permanent loss of active lithium inventory. However, the sharpness of this drop could also be contributed to by the delamination of the electrodes during the collapse of the inner jelly roll. For the cells at −20 °C, the rate of degradation is highest within the first 15 cycles, which overlaps with the largest drop in CE. Since no double plateau features are observed in the relaxation profile, we can assume that plating at this temperature is irreversible. Linking the CE data with the ageing data, we can see that irreversible plating has the biggest impact on the performance of these cells, whilst reversible plating may still contribute to the capacity delivery of the cell during operation due to the stripping behaviour of this deposited metal lithium.

Utilising various ex-situ imaging techniques, the outcome of the electrochemical analysis can be confirmed by studying the physical effects of sub-zero temperature ageing. A cell from each ageing condition was opened to examine the electrodes' condition post cycling. Examination of the graphite electrode was split into three regions: the outer jelly roll, the middle jelly roll and the inner jelly roll. These samples were compared using a combination of SEM and optical microscopy, as shown below. To enable representative analysis, an uncycled electrode was also harvested to identify deviations from a 'fresh' condition. During transfer from the glovebox to the sample stages of the imaging equipment, the samples were exposed to air and moisture. Despite this, many of the important and useful features of the metallic lithium layer remain visible in the resulting structure.

Fig. 5 compares SEM images of negative electrodes post ageing (*c,f,* and *i*), highlighting the significant differences in the state of the electrodes which occur due to the ageing of the cells. The images of the pristine electrode (see SI – Fig. S9) and the room temperature aged electrode are similar, with well dispersed particles typical of anode graphite particles seen in both. No significant cracking or microstructural degradation is visible in the ambiently aged cells, which is in keeping with the relatively small drop in capacity observed in the electrochemical cycling. In contrast, the images of the sub-zero temperature aged cells highlight significant deviations from conventionally aged cells. In both cells cycled at −10 °C and −20 °C (f) and i) respectively), the layers have a moss-like morphology which is more obvious at the edges of the layer fragments. These observations support the electrochemical results, with substantial evidence of a lithium layer across the negative electrode surface for the cold aged cells.

Fig. 5 highlights the progressive coverage of lithium plating as the temperature is lowered. After ageing at room temperature, it is possible to observe instances of small deposits of crystals accumulating around a nucleation point on the electrode. To find out whether these deposits are metallic lithium or dried electrolyte salts, elemental analysis would be required. However, most of the electrode surface is free from metallic lithium and available for lithium-ion intercalation. When examining the cells cycled at lower temperatures significant increases in plating can be seen, with almost full coverage of the graphite surface at −20 °C. Increasing the magnification reveals the morphology of these layers is more moss-like than dendritic, similar to the structures observed using SEM.

The optical images of the electrode surfaces provide insights on the extent of the electrode degradation. The contrast of the images indicates where the plating has predominantly occurred, with the lighter areas of the electrode having more plating than darker areas. Low magnification optical images (see the SI, Fig. S10) show a comparative view of the electrodes. The pristine and the room temperature aged electrodes appear identical on the macro scale, but at larger magnification there are multiple points of nucleation where plating has been initiated. This indicates that even under ambient temperatures lithium plating can occur during a relatively low number of cycles. The extent of plating can be seen to significantly increase as the ageing temperature is lowered. At −10 °C the lithium layer is seen to cover a considerable portion of the electrode surface; however, there are still regions where the thickness of lithium is much lower, identifiable by the darker colour. Examining the electrode at −20 °C, there is evidently more plating. The coverage of the light areas is more uniform and evenly spread (with a few notable dark regions).

The condition of the electrodes post-ageing is consistent with what was expected based on the electrochemical data where the cell performance is largely unaffected at room temperature, as shown by the similarity in appearance to the pristine anode sample. The physical

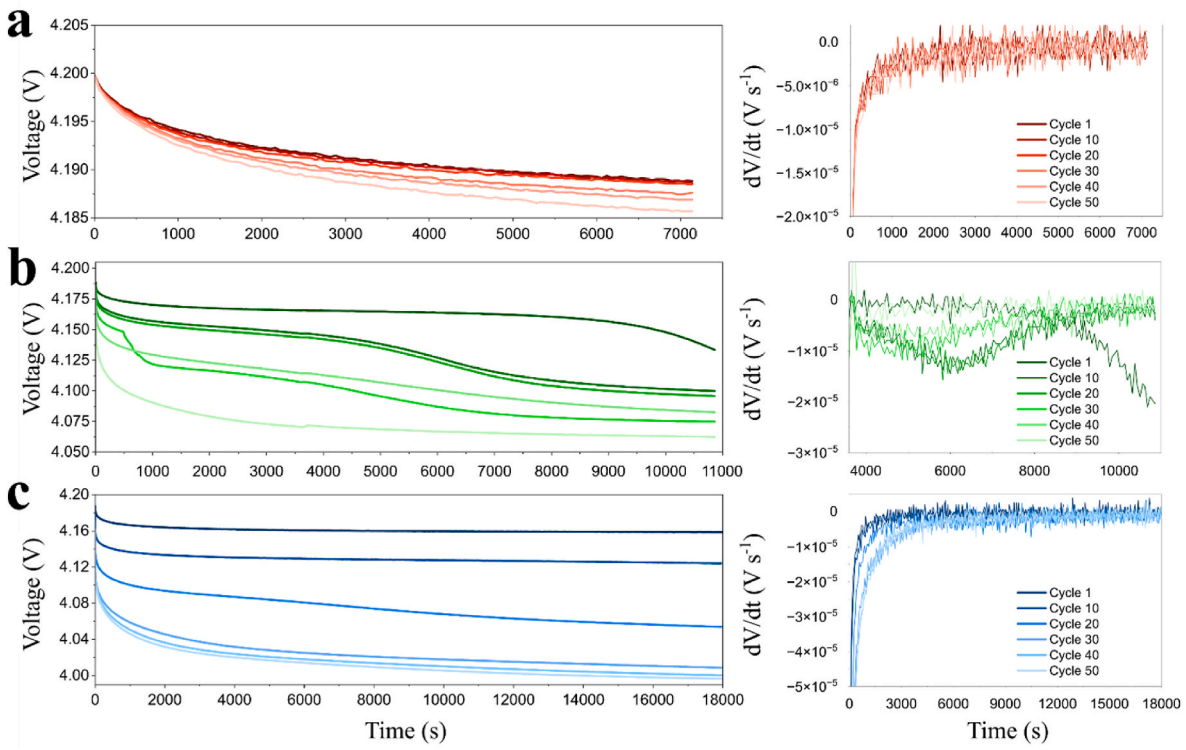

Fig. 4. The voltage relaxation profiles of the cells following charging. After reaching full charge, the cells were rested at open-circuit potential for 2 h at room temperature (a), 3 h at −10 °C (b), and 5 h at −20 °C (c), to account for the slower kinetics at lower temperatures. For each panel, the corresponding relaxation derivative (dV/dt) is provided on the right. Data are shown for representative cells from each ageing set (Cells 1, 4, and 7), with full datasets available in the Supporting Information (Fig. S7). It should be noted that the derivative relaxation plot for −10 °C (b) displayed significant noise between 0 and 3600 s and was therefore omitted here, with the full plot included in the Supporting Information (Fig. S8).

coverage of the lithium layers grows as temperature is lowered which reflects these cells' electrochemical performances.

To examine the internal structure of each cell before and after ageing, X-ray computed tomography was used with 3D reconstructions shown in Fig. 6.

Analysing scans of the cells post ageing, it is apparent that cycling at sub-zero temperatures causes significant internal deformation compared to operation at ambient conditions. The most obvious area of deformation is at the core of the cell, shown in Fig. 6. Electrode strain increases radially towards the centre of the cell due to winding tension, and the distribution of heat and pressure through the cell [52]. Heat, which is generated during cell operation and pressure from electrochemical expansion [52] and thermal expansion, due to elevated core temperatures, results in increased radial stress at the inner electrode layers [10,53,54]. The increased radial stress and elevated temperatures toward the centre of the cell create conditions that favour lithium deposition [22]. Higher internal pressure from the cell's winding tension and thermal expansion also compresses the electrode layers, increasing strain on the SEI. This can lead to SEI cracking, exposing fresh lithium sites where deposition can occur. Elevated temperatures accelerate these reactions, further encouraging lithium plating in these stressed regions, which amplifies the internal pressure and can destabilise the cell structure. Due to the absence of a central mandrel to support the structure of the jelly roll, the increased pressure on the layers causes them to collapse inwards [16,22]. As a result of this, the electrodes can delaminate and the central negative tab can twist, increasing the risk of a hard short, as well as lowering capacity by reducing the electrical contact between the active components. Fig. 6 also shows the condition of the cells cycled at room temperature which show little deformation with only a small amount of electrode delamination.

The electrode collapse appears to be marginally greater in the cells aged at −20 °C than those aged at −10 °C, which is due to the increased quantity of lithium deposited on the negative electrode surface. The length of the deformation was measured on Avizo (see example in SI, Fig. S12) and is summarised in the SI, Fig. S13. Another feature is that the extent of the deformation increases as we go up the cell from bottom to top. This is most likely due to the presence of the negative copper tab at the centre of the jelly roll. The tab is welded to the bottom of the cell casing and extends approximately 50 mm up the cell's length (70 mm). Thus, the inner electrodes at the top of the cell do not have a length of tab that needs pushing out of the way to release radial pressure via collapse. Furthermore, the collapse appears to be limited up to the layer in which the inner positive tab resides (Layer 13 in the case of this cell). We attribute this observation as a physical barrier rather than any electrochemical processes.

Accelerated rate calorimetry was employed to understand the impacts of sub-zero temperature degradation on the thermal stability and safety response to abusive temperatures of the cells. Fig. 7 highlights the thermal response of the aged cells to increasing temperature. A heat-wait-search protocol is applied to the cells over increments of 5 °C which allows us to identify any features of self-heating or venting. These events are characterised by an increase in temperature during the wait step of the heating protocol or a drop in temperature during heating, respectively.

From the temperature profiles, we can extract some key safety parameters, such as the heating rate (°C min^{-1}) onset temperature of self-heating (T_{SH}), the thermal runaway temperature (T_{TR}) and the maximum temperature reached (T_{max}). This information has been summarised in Table 2. The onset of self-heating starts with the breakdown of the SEI layer, which typically begins to happen at *ca.* 90–130 °C [55]. Once this layer is compromised, the intercalated lithium is exposed to the electrolyte and reacts exothermically in a more uncontrolled manner than during formation to drive the temperature up even more [56]. Above a certain temperature, typically 100 °C, this decomposition

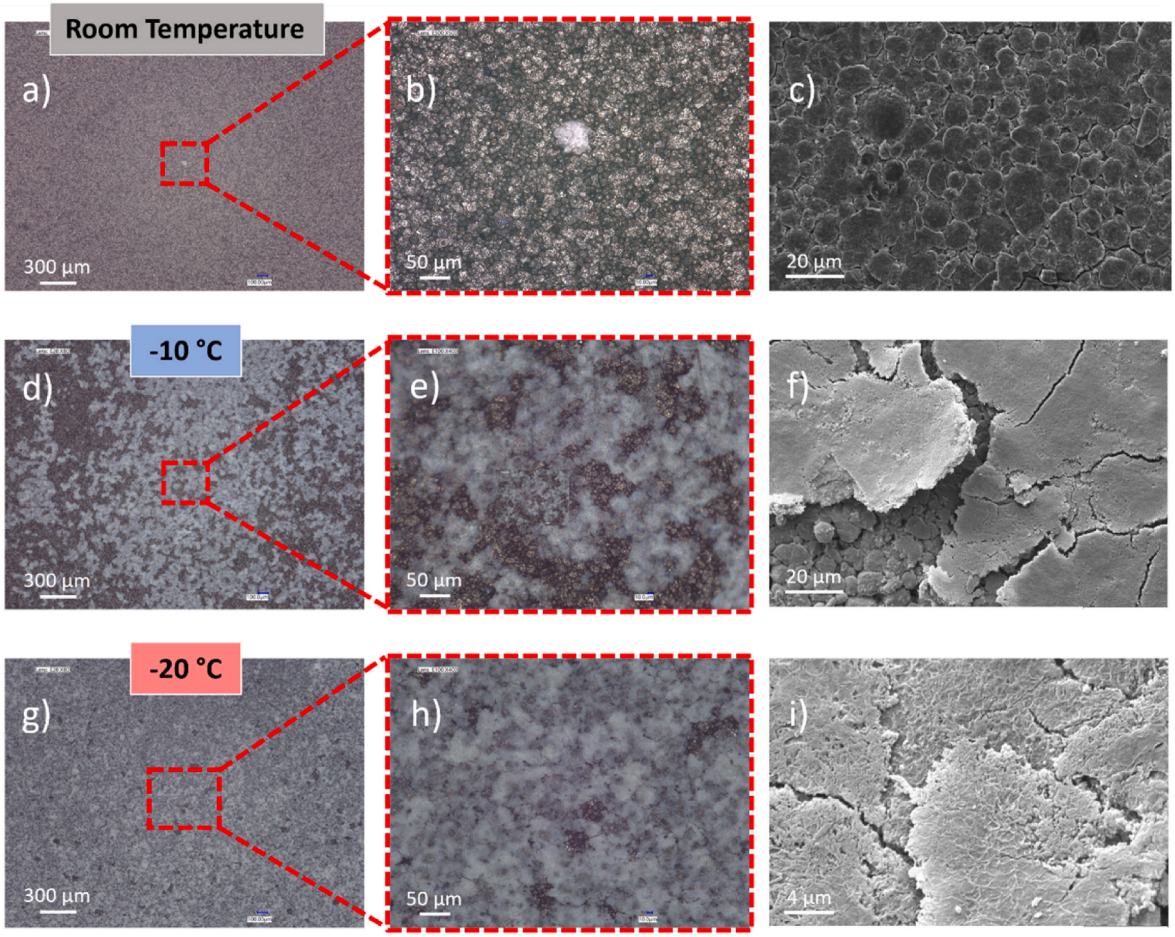

Fig. 5. Optical microscopy and SEM images of the electrodes after each ageing condition: (a–c) room temperature, (d–f) −10 °C, and (g–i) −20 °C. The images in the far-right column (c, f, and i) correspond to SEM, while the others were obtained using optical microscopy.

reaction causes the release of flammable hydrocarbons, such as ethane, methane, ethylene, etc [57]. This feedback loop generates more heat until the temperature exceeds the melting point of the separator (130–165 °C) allowing for short circuits to occur [56]. This and the heat generation increases the temperature high enough to start decomposing the metal oxide cathode material releasing oxygen enabling the flammable gases within the cell to combust [56]. This is usually the point at which thermal runaway starts to occur. However, with the presence of metallic lithium, this process occurs sooner and at a faster rate. Lithium metal has a lower potential than LiC_6 (the fully lithiated form of graphite) and is chemically more reactive which means reduction of common electrolytes (such as ethylene carbonate) is more energetically favourable than in cells without plating [58]. In addition to this, the reaction results in the generation of CO gas unlike decomposition in contact with graphite surfaces [59]. This can substantially increase the internal pressure within the cell.

The cell aged at −20 °C exhibits a much earlier onset of self-heating, 110 °C, than the cell at cycled at room temperature, 160 °C. This early onset of self-heating is due to the substantial amount of lithium plating seen on the negative electrodes of the cells aged at this temperature, in the process described above. Interestingly, we see a later start to self-heating, 174 °C, in the cell aged at −10 °C which is not expected since there is most likely to also be metallic lithium deposited on the graphite surface of this cell. This degree of thermal stability is somewhat unexpected in a cell exhibiting extensive lithium plating on the negative electrode. One possible explanation is that repeated reactions between metallic lithium and the electrolyte have led to the formation of a thicker, more passivating interphase layer around the plated lithium. As a result, the metallic lithium may only decompose the innermost, older SEI layers, while the newer SEI products—formed more recently and under milder conditions—remain intact. These freshly formed SEI layers may be more stable and effective at insulating the lithium from direct contact with the electrolyte. This would suppress further parasitic reactions and limit additional gas evolution or heat release, thereby maintaining overall thermal stability despite the presence of reactive lithium. It should be noted that this observation may not be statistically significant and could represent an outlier as failure is a dynamic phenomenon that can present different behaviours under the same experimental conditions.

The onset of thermal runaway, T_{TR}, is defined, by Buckwell et al., as the point at which the self-heating rate exceeds 100 °C min^{-1} [60]. At this point the cascade of exothermic decomposition reactions elevates the temperature rapidly, resulting in catastrophic failure. In relation to this specific failure metric, all three cells exhibited comparable behaviour, with thermal runaway initiating at approximately 200 °C. This consistency can be attributed to the fundamental nature of the reactions governing the onset of thermal runaway. As discussed earlier, metallic lithium primarily influences the temperature at which the solid electrolyte interphase (SEI) and electrolyte decompose. However, the critical failure points—such as separator meltdown and cathode decomposition—occur independently of the presence or extent of lithium plating. These events are primarily driven by intrinsic material properties and thermal thresholds, such as the melting point of the polymer separator and the oxygen release from cathode materials at elevated temperatures. Therefore, while lithium plating may exacerbate other failure modes (e.g. gas generation, impedance growth), it has

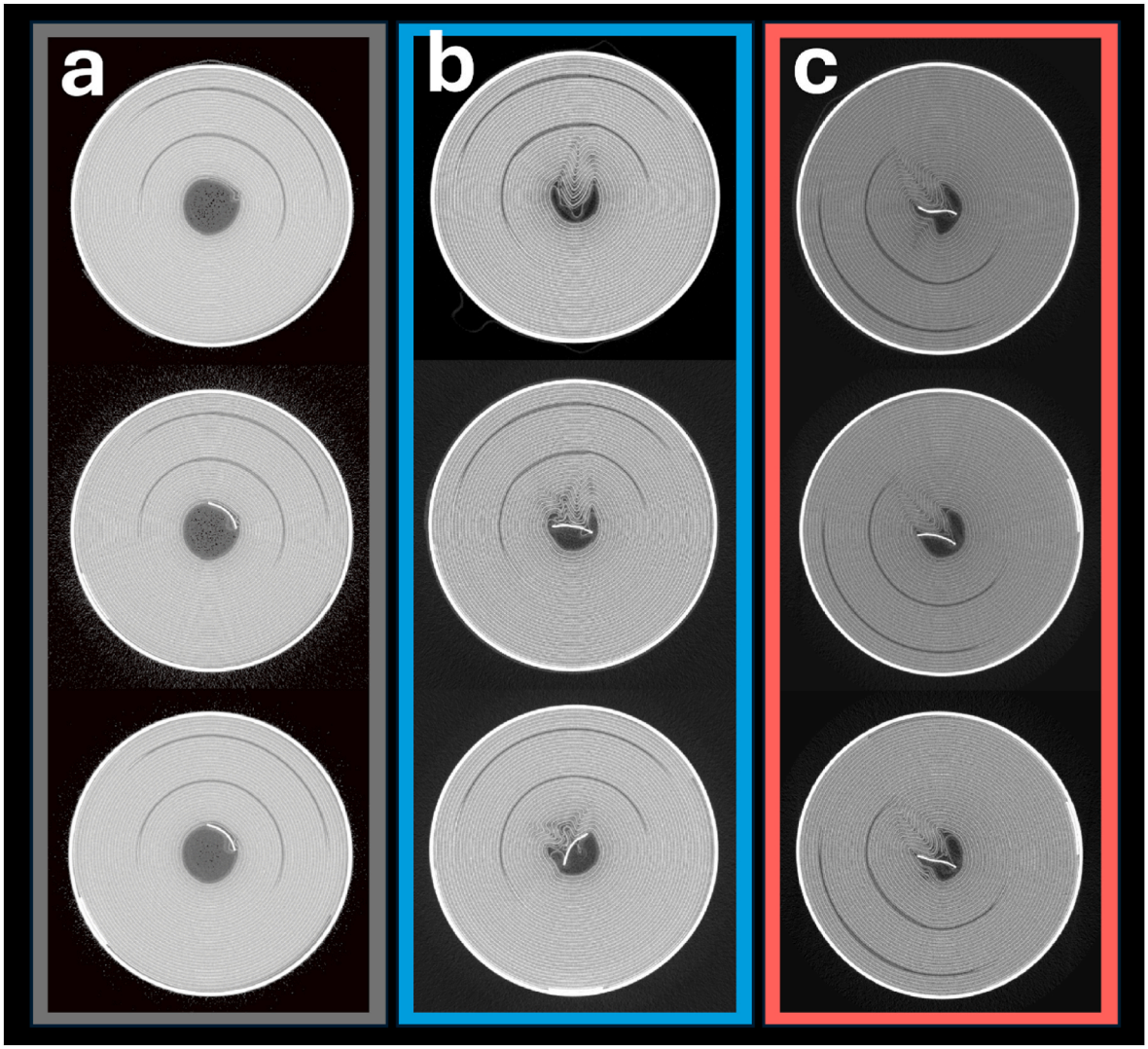

Fig. 6. X-ray macro-CT results of the 21700 cells after cycling: (a) Cell 1 aged at room temperature, (b) Cell 4 aged at −10 °C, and (c) Cell 7 aged at −20 °C. These three cells were selected as representative of their respective ageing sets. The full dataset is provided in the SI (Fig. S11).

minimal influence on the specific temperature at which thermal runaway is triggered.

T_{max} is the biggest differential of thermal behaviour between the aged cells. As discussed previously, when exposed to high temperatures the presence of lithium plating causes an increased severity of decomposition reactions with the electrolyte. Thus, the cells that are aged at colder temperatures will experience higher internal pressures during thermal runaway. This results in the ejection of active material during venting or rupture events, as reported by Waldmann et al. [61,62]. This is highlighted in the post-mortem X-ray CT scans, see Fig. 8. Therefore, with a greater extent of plating we can expect an increased potential for the ejection of active material during failure due to the higher internal pressures from the gas producing decomposition pathways that metallic lithium causes. As more of the cells contents is ejected, the T_{max} decreases as less active material remains in the cell to be consumed by the reaction fuelling thermal runaway. However, the results for this are not consistent with the trends for T_{SH} and T_{TR}, suggesting that more data is needed to reach a full conclusion on how these parameters are affected by lithium plating.

Following the ARC testing of the aged cells, post-mortem X-ray CT was performed as a forensic tool to provide insights into the dynamics of these failures. By looking at the distribution of material (or lack thereof) we can gain information about how the thermal runaway event propagated to better explain the thermal stability parameters found in the ARC investigations.

Post-mortem scans of cell 1, see Fig. 8a, reveal the presence of copper globules, indicating that the internal temperature of the cell exceeded 1085 °C (the melting point of copper) [63]. These globules are only found in the top half of the cell, with a large void space occupying the bottom of the cell. This is most likely due to the build-up of internal pressure during the exothermic decomposition of the active materials causing the electrode assembly to displace towards the cap as the cell vents or ruptures due to thermal runaway. Finegan et al. showed that the location of thermal runaway initiation can also influence the dynamics of failure. Initiation at the bottom of the cell can result in the ejection of intact contents, whereas failure originated from the top of the cell can propagate down the electrode assembly [63]. Linking this back to the X-ray CT scans of the aged cells, we see that there is less severe deformation of the bottom tab. This is close to where it is welded to bottom of the casing, thus providing increased structural stability than the section of tab further up the cell. This increased stability at the bottom of the cell means that the expansion of the electrode layers is resisted more, possibly increasing the likelihood of a hard short occurring due to piercing of the electrode layers by the tab. Meanwhile, the movement of this material causes a negative pressure at the bottom of the cell which results in air from the cell surroundings to be sucked in to equalise this

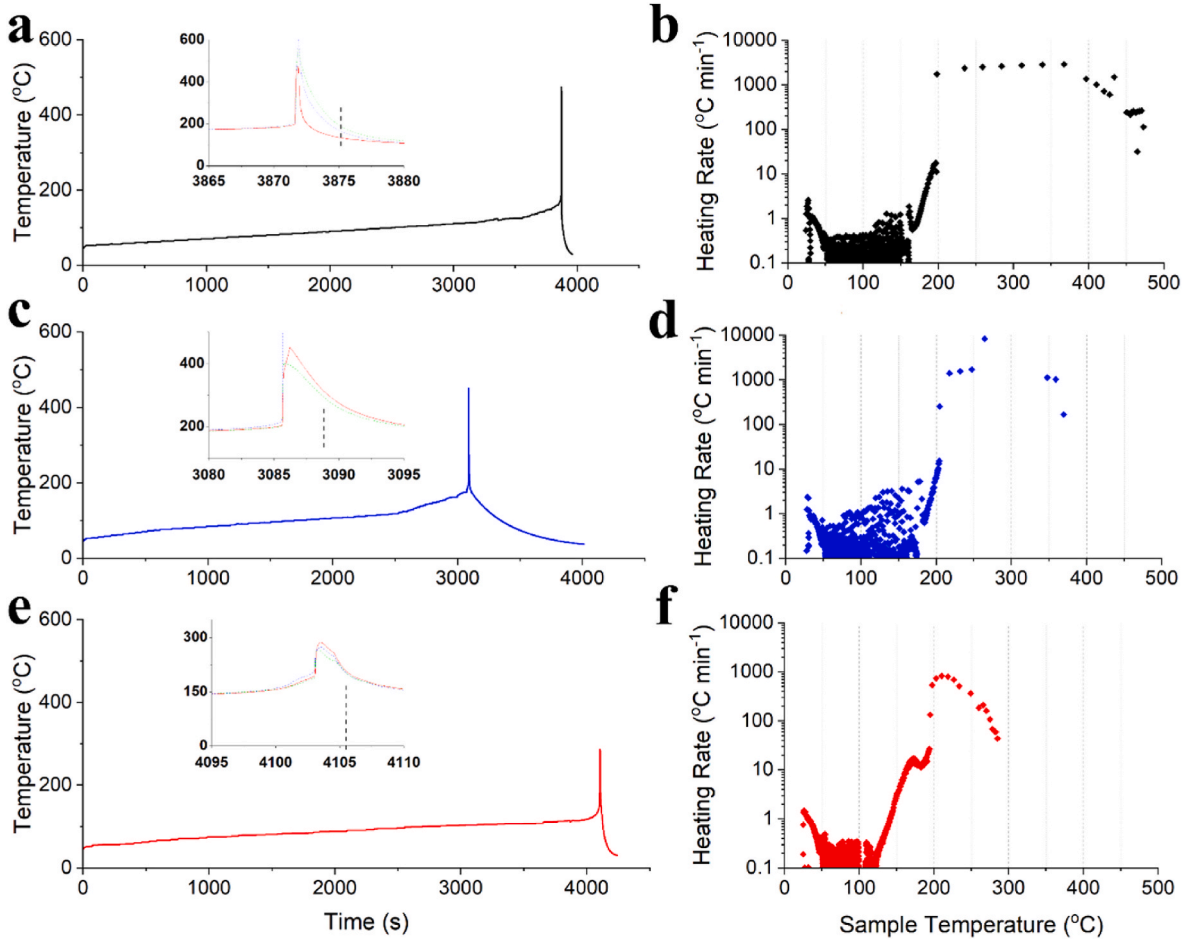

Fig. 7. Accelerating rate calorimetry (ARC) profiles obtained under a heat–wait–search protocol. The starting temperature was 50 °C and increased in 5 °C increments. The left panels show the temperature evolution of the cells during heating, while the right panels show the corresponding heating rates. Cell 1 (aged at room temperature) is presented in the top row, Cell 4 (aged at −10 °C) in the middle row, and Cell 7 (aged at −20 °C) in the bottom row. The primary temperature profiles are taken from the thermocouple placed on the body of the cell, as this most accurately reflects the internal temperature. Above each curve, thermal runaway snapshots are provided, with temperature traces from all three thermocouple positions (cap, body, and base) included.

Table 2
Key parameters from the ARC measurements are summarised: the peak temperature during thermal runaway (T_{max}), the onset temperature of self-heating (T_{SH}), and the temperature at which thermal runaway occurs (T_{TR}). For Cell 1, the maximum temperature was recorded by the thermocouple placed at the cap of the cell rather than the body, and this value has therefore been reported as T_{max}.

Cell	Ageing temperature (°C)	Cycle Life	Capacity (%)	T_{SH} (°C)	T_{TR} (°C)	T_{max} (°C)
Cell 1	25	50	95	160	198	599
Cell 4	−10	50	76	175	204	452
Cell 7	−20	50	29	114	194	287

pressure gradient. As this air is supplied to the reacting active material, the oxygen present further fuels thermal runaway which can generate more heat within the cell [63]. The displaced active material also appears to have blocked the cap which could have allowed the cell to reach such high temperatures as the active material is therefore retained and the reaction has more fuel to burn.

Comparing the post-mortem scans of the cells aged at subzero temperatures, we find a lack of copper globules within the remaining material which indicates that the internal temperatures did not exceed copper's melting point. These lower temperatures are likely due to a combination of the low capacity of the cells and the increased ejection of active material observed in these failures. As discussed before, cells that have a greater amount of plated lithium on the surface of the graphite electrode undergo more significant decomposition reactions that result in gas generation, thus causing these cells to reach higher internal pressures. The X-ray CT scans reveal considerably more void space at the bottom but also axially in the cell aged at room temperature. This indicates that more of the active material was ejected from the cell during thermal runaway and therefore left less material to combust and generate heat from. This is highlighted by the difference of recorded T_{max} between the cells aged at −10 °C and −20 °C, the latter having completely ejected its electrode assembly, which resulted in a lower maximum temperature than the cell at −10 °C which only partially ejected its active material. Since the capacities of these cells were relatively similar after ageing, it indicates that the ejection of active material is the primary influence for the lower maximum temperatures observed in the cell at −20 °C.

These findings indicate that with increased lithium plating, cells have a greater projectile potential. Additional repeats are needed to solidify these findings and give the data statistical relevance. This has significant implications for safety as these projectiles can cause harm if ejected towards an individual. Additionally, there is the potential for this ejected material to still be burning or reacting and thus capable of generating heat which could propagate the failure to neighbouring cells

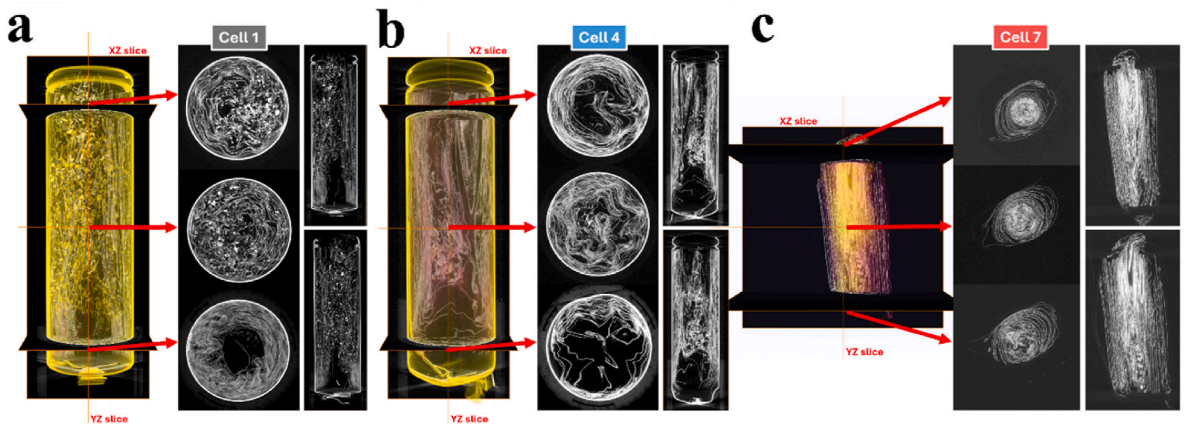

Fig. 8. Post-mortem X-ray macro-CT results of the cells aged at room temperature (a), −10 °C (b), and −20 °C (c). 3D reconstructions, along with XY, XZ, and YZ orthogonal slices, reveal the internal structural changes following cell failure.

if the ejecta contacts the cell itself.

4. Conclusions

The electrochemical data from the ageing regimes underlines the negative impact that lithium plating has on cell performance. Excessive losses in capacity and CEs highlight how reducing the temperature of operation exacerbates the extent of plating, thus the decay in nominal function. Monitoring voltage relaxation behaviour and CEs, it was possible to identify a correlation between temperature and the reversibility of plating. Through the relaxation profiles, ageing at −10 °C showed evidence of stripping (reversible plating) behaviour that declined with ageing. Observing the CEs, the ageing groups showed drops in efficiency at different times. Cells aged at −20 °C fell early on in ageing, implying plating was mostly irreversible throughout, whereas the drop came after the reduction in the double plateau feature, indicating that irreversible plating became more prominent later during ageing. EIS measurements support this idea, as the resistance of the cells rises most significantly where decreases in CE are also highest. This suggests that the nature of plating is dependent on temperature and looking into where this threshold of behaviour lies and how it can impact ambient cell recovery will be beneficial to investigate.

Ex-situ characterisation confirmed the results of the electrochemical analysis, showing an increased coverage of deposited lithium over the graphite electrode surface as the temperature of operation is reduced.

Post-ageing, macro-X-ray CT imaging revealed that significant mechanical deformation was present in the cells aged at sub-zero temperatures. Delamination and loss of structural integrity will ultimately contribute to capacity fade and tracking this deformation behaviour alongside the capacity data will be important in knitting our understanding of how much this affects the cell performance. As well as this, the scans also highlight how deformation of this nature can increase the risk of a hard short, which is a safety concern.

ARC testing showed that the cells aged at −20 °C have significantly reduced self-heating and thermal runaway temperatures than cells aged in ambient conditions. The stronger exothermic reactions of the metallic lithium cause decomposition to occur earlier and via a pathway that increases the amount of gas evolution – emphasised by the jelly roll collapse. This leads to a more energetic failure dynamic which results in the projection of a significant proportion of the active material which in turn results in lower maximum temperatures. Despite these results, there exists some discrepancies with the results seen in the intermediate temperature cells (at −10 °C) that need revisiting to fully understand how thermal stability is affected by lithium plating. Post-mortem CT scans support these findings by revealing the distribution of material remaining in the cell casing after failure.

Studies on linking the internal structural collapse to the initiation location of thermal runaway using synchrotron facilities are being conducted and will further highlight the significance of the electrode collapse to cell safety and add to this work.

CRediT authorship contribution statement

Charles Kirchner-Burles: Writing – original draft, Investigation, Formal analysis, Data curation, Conceptualization. **Arthur Fordham:** Writing – review & editing, Investigation, Data curation. **Hamish T. Reid:** Writing – review & editing, Investigation, Data curation. **Michael Johnson:** Writing – review & editing, Investigation, Data curation. **Mark Buckwell:** Writing – review & editing, Investigation, Data curation. **Francesco Iacoviello:** Writing – review & editing, Investigation, Data curation. **Kofi Coke:** Writing – review & editing, Investigation, Data curation. **Rhodri Jervis:** Writing – review & editing, Supervision, Resources, Methodology, Formal analysis, Conceptualization. **Gareth Hinds:** Writing – review & editing, Supervision, Resources, Methodology, Formal analysis, Conceptualization. **Paul R. Shearing:** Writing – original draft, Supervision, Methodology, Investigation, Funding acquisition, Formal analysis, Conceptualization. **James B. Robinson:** Writing – original draft, Supervision, Resources, Methodology, Funding acquisition, Formal analysis, Conceptualization.

Declaration of competing interest

The authors declare no further interests.

Acknowledgements

The authors would like to acknowledge Innovate UK and the Aerospace Technology Institute for funding through the CEBD programme (10050803). Shearing, Jervis and Robinson would like to acknowledge the Safebatt, LiSTAR and Degradation projects and the wider support of the Faraday Institution (www.faraday.ac.uk; EP/S003053/1, FIRG058, FIRG060, FIRG061).https://www.safebatt.ac.uk/ Shearing also acknowledges the Royal Academy of Engineering Chair in Emerging Technologies (CiET1718\59). CKB would also like to acknowledge support from the National Measurement System of the UK Department of Science, Innovation and Technology. Johnson acknowledges HORIBA-MIRA, UCL, EPSRC (EP/R513143/1) and Dr. Alex Rettie for a CASE studentship.

Appendix A. Supplementary data

Supplementary data to this article can be found online at https://doi.

org/10.1016/j.jpowsour.2025.238565.

Data availability

Data will be made available on request.

References

[1] B. Scrosati, J. Garche, Lithium batteries: status, prospects and future, J. Power Sources 195 (2010) 2419–2430.
[2] Aurbach, D., Zinigrad, E., Cohen, Y. & Teller, H. A Short Review of Failure Mechanisms of Lithium Metal and Lithiated Graphite Anodes in Liquid Electrolyte Solutions.
[3] J. Jaguemont, L. Boulon, Y. Dubé, A Comprehensive Review of lithium-ion Batteries Used in Hybrid and Electric Vehicles at Cold Temperatures, 2015, https://doi.org/10.1016/j.apenergy.2015.11.034.
[4] N. Piao, et al., Challenges and development of lithium-ion batteries for low temperature environments, eTransportation 11 (2022) 100145.
[5] C.R. Birkl, M.R. Roberts, E. McTurk, P.G. Bruce, D.A. Howey, Degradation diagnostics for lithium ion cells, J. Power Sources 341 (2017) 373–386.
[6] J.P. Pender, et al., Electrode degradation in lithium-ion batteries, ACS Nano 14 (2020) 1243–1295.
[7] X. Han, et al., A review on the key issues of the lithium ion battery degradation among the whole life cycle, eTransportation 1 (2019) 100005.
[8] J.S. Edge, et al., Lithium ion battery degradation: what you need to know, Phys. Chem. Chem. Phys. 23 (2021) 8200–8221.
[9] J. Zhu, T. Wierzbicki, W. Li, A review of safety-focused mechanical modeling of commercial lithium-ion batteries, J. Power Sources 378 (2018) 153–168.
[10] M.D.R. Kok, et al., Tracking the lifecycle of a 21700 cell: a 4D tomography and digital disassembly study, J. Electrochem. Soc. 170 (2023) 090502.
[11] T. Waldmann, et al., A mechanical aging mechanism in lithium-ion batteries, J. Electrochem. Soc. 161 (2014) A1742–A1747.
[12] R.V. Bugga, M.C. Smart, Lithium plating behavior in lithium-ion cells, ECS Trans. 25 (2010) 241–252.
[13] Q. Liu, et al., Understanding undesirable anode lithium plating issues in lithium-ion batteries, RSC Adv. 6 (2016) 88683–88700.
[14] X. Lin, K. Khosravinia, X. Hu, J. Li, W. Lu, Lithium plating mechanism, detection, and mitigation in lithium-ion batteries, Prog. Energy Combust. Sci. 87 (2021) 100953.
[15] M. Petzl, M.A. Danzer, Nondestructive detection, characterization, and quantification of lithium plating in commercial lithium-ion batteries, J. Power Sources 254 (2014) 80–87.
[16] R. Carter, E.J. Klein, R.W. Atkinson, C.T. Love, Mechanical collapse as primary degradation mode in mandrel-free 18650 Li-ion cells operated at 0 °C, J. Power Sources 437 (2019) 226820.
[17] R. Xiong, S. Ma, H. Li, F. Sun, J. Li, Toward a safer battery management system: a critical review on diagnosis and prognosis of battery short circuit, iScience 23 (2020) 101010.
[18] G. Zhang, et al., Internal short circuit mechanisms, experimental approaches and detection methods of lithium-ion batteries for electric vehicles: a review, Renew. Sustain. Energy Rev. 141 (2021) 110790.
[19] Z. Chen, R. Xiong, F. Sun, Research status and analysis for battery safety accidents in electric vehicles, Jixie Gongcheng Xuebao/J. Mech. Eng. 55 (2019).
[20] S. Santhanagopalan, P. Ramadass, J. Zhang, (Zhengming). Analysis of internal short-circuit in a lithium ion cell, J. Power Sources 194 (2009) 550–557.
[21] Y. Li, et al., Thermal runaway triggered by plated lithium on the anode after fast charging, ACS Appl. Mater. Interfaces 11 (2019) 46839–46850.
[22] B. Ng, et al., Low-temperature lithium plating/corrosion hazard in lithium-ion batteries: electrode rippling, variable states of charge, and thermal and nonthermal runaway, ACS Appl. Energy Mater. 3 (2020) 3653–3664.
[23] D.P. Finegan, et al., Investigating lithium-ion battery materials during overcharge-induced thermal runaway: an operando and multi-scale X-ray CT study, Phys. Chem. Chem. Phys. 18 (2016) 30912–30919.
[24] X. Feng, D. Ren, X. He, M. Ouyang, Mitigating thermal runaway of lithium-ion batteries, Joule 4 (2020) 743–770.
[25] T. Waldmann, B.I. Hogg, M. Wohlfahrt-Mehrens, Li plating as unwanted side reaction in commercial Li-ion cells – a review, J. Power Sources 384 (2018) 107–124.
[26] J. Jaguemont, L. Boulon, Y. Dubé, A comprehensive review of lithium-ion batteries used in hybrid and electric vehicles at cold temperatures, Appl. Energy 164 (2016) 99–114.
[27] G. Sarre, P. Blanchard, M. Broussely, Aging of lithium-ion batteries, J. Power Sources 127 (2004) 65–71.
[28] M. Petzl, M. Kasper, M.A. Danzer, Lithium plating in a commercial lithium-ion battery - a low-temperature aging study, J. Power Sources 275 (2015) 799–807.
[29] N. Gunawardhana, et al., Suppression of lithium deposition at sub-zero temperatures on graphite by surface modification, Electrochem. Commun. 13 (2011) 1116–1118.
[30] G. Zhang, et al., Lithium plating on the anode for lithium-ion batteries during long-term low temperature cycling, J. Power Sources 484 (2021) 229312.
[31] M. Kaliaperumal, et al., Cause and mitigation of lithium-ion battery failure—A review, Materials 2021 14 (2021) 5676, 14, 5676.
[32] Z. Li, R. Fang, H. Ge, Investigation of Lithium Plating-Stripping Process in Li-Ion Batteries at Low Temperature Using an Electrochemical Model you May Also like Multiphysics Footprint of Li Plating for Li-Ion Battery and Challenges for High-Accuracy Detection, 2018, https://doi.org/10.1149/2.0661810jes.
[33] X. Zhao, Y. Yin, Y. Hu, S.-Y. Choe, Electrochemical-Thermal Modeling of Lithium plating/stripping of Li (Ni 0.6 Mn 0.2 Co 0.2)O 2/Carbon lithium-ion Batteries at Subzero Ambient Temperatures, 2019, https://doi.org/10.1016/j.jpowsour.2019.02.001.
[34] C. Uhlmann, J. Illig, M. Ender, R. Schuster, E. Ivers-Tiffée, In situ detection of lithium metal plating on graphite in experimental cells, J. Power Sources 279 (2015) 428–438.
[35] S. Schindler, M. Bauer, M. Petzl, M.A. Danzer, Voltage relaxation and impedance spectroscopy as in-operando methods for the detection of lithium plating on graphitic anodes in commercial lithium-ion cells, J. Power Sources 304 (2016) 170–180.
[36] C. von Lüders, et al., Lithium plating in lithium-ion batteries investigated by voltage relaxation and in situ neutron diffraction, J. Power Sources 342 (2017) 17–23.
[37] J.C. Burns, D.A. Stevens, J.R. Dahn, In-Situ detection of lithium plating using high precision coulometry, J. Electrochem. Soc. 162 (2015) A959–A964.
[38] Y. Tian, C. Lin, H. Li, J. Du, R. Xiong, Detecting undesired lithium plating on anodes for lithium-ion batteries – a review on the in-situ methods, Appl. Energy 300 (2021) 117386.
[39] M. Petzl, M. Kasper, M.A. Danzer, Lithium plating in a commercial lithium-ion battery – a low-temperature aging study, J. Power Sources 275 (2015) 799–807.
[40] M. Zhao, et al., Electrochemical stability of copper in lithium-ion battery electrolytes, J. Electrochem. Soc. 147 (2000) 2874.
[41] A. Nazari, S. Farhad, Heat generation in lithium-ion batteries with different nominal capacities and chemistries, Appl. Therm. Eng. 125 (2017) 1501–1517.
[42] G. Kucinskis, et al., Arrhenius plots for Li-ion battery ageing as a function of temperature, C-rate, and ageing state – an experimental study, J. Power Sources 549 (2022) 232129.
[43] M. Safari, M. Morcrette, A. Teyssot, C. Delacourt, Multimodal physics-based aging model for life prediction of Li-Ion batteries, J. Electrochem. Soc. 156 (2009) A145.
[44] M. Broussely, et al., Main aging mechanisms in Li ion batteries, J. Power Sources 146 (2005) 90–96.
[45] W.J. Dawson, et al., The effect of mud cracking on the performance of thick Li-ion electrodes, Batter Supercaps (2024) e202400260, https://doi.org/10.1002/BATT.202400260.
[46] Y. Ji, Y. Zhang, C.-Y. Wang, Li-Ion cell operation at low temperatures, J. Electrochem. Soc. 160 (2013) A636–A649.
[47] D.J. Yoo, et al., Understanding the role of SEI layer in low-temperature performance of lithium-ion batteries, ACS Appl. Mater. Interfaces 14 (2022) 11910–11918.
[48] Z. Chen, et al., Overpotential analysis of graphite-based Li-ion batteries seen from a porous electrode modeling perspective, J. Power Sources 509 (2021) 230345.
[49] S. Yang, et al., Minimum lithium plating overpotential control based charging strategy for parallel battery module prevents side reactions, J. Power Sources 494 (2021) 229772.
[50] L. Pei, T. Wang, R. Lu, C. Zhu, Development of a voltage relaxation model for rapid open-circuit voltage prediction in lithium-ion batteries, J. Power Sources 253 (2014) 412–418.
[51] L. Chen, et al., Review—lithium plating detection methods in Li-Ion batteries, J. Electrochem. Soc. 167 (2020) 160552.
[52] S.P.V. Nadimpalli, V.A. Sethuraman, D.P. Abraham, A.F. Bower, P.R. Guduru, Stress evolution in lithium-ion composite electrodes during electrochemical cycling and resulting internal pressures on the cell casing, J. Electrochem. Soc. 162 (2015) A2656–A2663.
[53] J. Chen, et al., Stress and displacement of cylindrical lithium-ion power battery during charging and discharging, Energies 2022 15 (2022) 8244. *Page 8244* **15**.
[54] M.D.R. Kok, et al., Virtual unrolling of spirally-wound lithium-ion cells for correlative degradation studies and predictive fault detection, Sustain. Energy Fuels 3 (2019) 2972–2976.
[55] X. Mi, H. Li, X. Huang, Thermal behavior of lithiated graphite with electrolyte in lithium-ion batteries you may also like study of various ('Super iron') MFeO 4 compounds in Li salt solutions as potential cathode materials for Li batteries maxim koltypin, in: Stuart Licht, Israel Nowik, et al. (Eds.), Carbon-Coated Li 1.2 Cr 0.4 Ti 0.4 O 2 Cathode Material for Lithium-Ion Batteries, 2005, https://doi.org/10.1149/1.2139955.
[56] Q. Wang, et al., Thermal runaway caused fire and explosion of lithium ion battery, J. Power Sources 208 (2012) 210–224.
[57] Spotnitz, R. & Franklin, J. Abuse Behavior of high-power, lithium-ion Cells.
[58] A. Wang, S. Kadam, H. Li, S. Shi, Y. Qi, Review on modeling of the anode solid electrolyte interphase (SEI) for lithium-ion batteries, npj Comput. Mater. 2018 4 (2018) 1–26, 1 4.
[59] M. Ebadi, D. Brandell, C.M. Araujo, Electrolyte decomposition on Li-metal surfaces from first-principles theory, J. Chem. Phys. 145 (2016) 204701.
[60] M. Buckwell, et al., Failure and hazard characterisation of high-power lithium-ion cells via coupling accelerating rate calorimetry with in-line mass spectrometry, statistical and post-mortem analyses, J. Energy Storage 65 (2023) 107069.
[61] M. Fleischhammer, T. Waldmann, G. Bisle, B.€O.-I. Hogg, M. Wohlfahrt-Mehrens, Interaction of Cyclic Ageing at high-rate and Low Temperatures and Safety in lithium-ion Batteries, 2014, https://doi.org/10.1016/j.jpowsour.2014.08.135.
[62] T. Waldmann, M. Wohlfahrt-Mehrens, Effects of rest time after Li plating on safety behavior—Arc tests with commercial high-energy 18650 Li-ion cells, Electrochim. Acta 230 (2017) 454–460.
[63] D.P. Finegan, et al., In-operando high-speed tomography of lithium-ion batteries during thermal runaway, Nat. Commun. 2015 6 (2015) 1–10, 1 6.